# Validated numerical simulation of airflow in child respiratory airways

Miloslav *Belka*[1*], *Milan* Maly[1], *Ondrej* Cejpek[1], *Jakub* Elcner[1], *Frantisek* Lizal[1], *Jan* Jedelsky[1] and *Miroslav* Jicha[1]

[1]Brno University of Technology, Department of thermodynamics and environmental sciences, 616 69 Brno, Czech Republic

**Abstract.** Both pulmonary airway geometry and breathing pattern evolve from birth to adulthood. These gradual changes significantly influence airflow dynamics and subsequently particle transport and deposition. Regarding the airway structure, the differences between infants and adults are most profound till 5 years of age. Since that age the child airway geometry can be downsized from adult lungs. The objective of the present work was to investigate airflow patterns in child airways. The digital model of male respiratory airways was downsized to dimensionally correspond to a 5–year old child. Airflow simulations with properly validated RANS k–ω turbulence model were performed under steady inhalation boundary conditions. The inspiratory flow rate was 12.5 L/min. The velocity profiles just upstream of the first bifurcation were validated by Laser–Doppler anemometry (LDA) experiments. A replica of the same geometry as the one used in the simulation was 3D printed and part of the trachea was replaced by a glass tube. LDA measurements in several points upstream of the first bifurcation were carried out. The validated flow patterns were compared to the ones obtained in adult lungs.

## 1. Introduction

According to [1], about 300 million children worldwide breath polluted air that exceeds international guidelines sixfold. The effects of indoor and outdoor pollution cause nearly 600 000 deaths of children under 5 years old every year [1]. Moreover, an early life respiratory illnesses and exposure to pollutants were correlated with increased risk of airway obstructions [2] and asthma [3] in adulthood. Children are more vulnerable to polluted air compared to adults due to their weaker immune system and higher respiratory rates taking in more air relative to their body weight. Also, the narrow airway calibre is more susceptible to obstructions from any inflammatory disease [4].

Therefore, the research of particulate matter transport and deposition in juvenile population is crucial. Although a lot of attention was paid to healthy adults, children received less interest. One of the reasons is the limited access of researchers to pediatric medical images [5]. It is also not entirely possible to extrapolate results from adults to children as there are differences in lung morphology and breathing regimes affecting the subsequent airflow dynamics [6].

Respiratory airways continue to develop after birth and the changes are rapid until the age of roughly 5 years. During this period the airways change not just in dimensions but also in shape, e.g. 4–month–old subject has shorter nasal turbine region and narrower nasopharynx compared to adults [5]. Since age of 5 years the respiratory airways can be down-scaled from adult lungs with reasonable accuracy [7]. The breathing patterns differ significantly from adults as well. Up to the age of 20 months the nasal breathing is preferential. Also, tidal volume is lower and respiratory rate is higher compared to adults [4].

Because of ethical and practical reasons, it is not feasible to study particulate matter transport and deposition in children using *in* vivo methods. However, there has been a significant progress in various *in silico* models, such as the use of computational fluid dynamics to solve equations of fluid flow and particle movement. The geometry used in these simulations can be both idealized or realistic. Tsega [8] analysed numerically airflow differences between infant, child, and adult in idealized symmetric geometries of tracheobronchial airways, in particular G3–G6 and G9–G12. It was found that velocity, pressure and wall shear stress decreases with increasing age indicating that infants are more susceptible to airway damages. Deng et al. [9] investigated deposition in the same parts of the tracheobronchial airways in infant, child and adult. The deposition efficiency decreased with increasing age showing that infants and children are more vulnerable to harmful effects of pollutants. Apart from idealized models, realistic geometries can be based on CT scans. Oakes et al. [6] created subject–specific models of infant, child and adult. They carried out simulations of entire respiratory cycle and highlighted dissimilarities between age–dependent peak pressure drops and velocities. Xi et al. [5] developed several upper respiratory airway models spanning the period from infancy (4–month–old) to childhood (5–year–old). The models were compared and employed in CFD simulations. The influence of age and airway

* Corresponding author: belka@fme.vutbr.cz

abnormalities on pressure drop and regional aerosol deposition were described.

The aforementioned studies focused on either upper airways or tracheobronchial tree. However, it is essential to include both regions to accurately describe the flow features as the flow through upper respiratory and glottis is quite complex and its influence propagates downstream to at least first bifurcation [10]. Moreover, the models need experimental validation. This validation should be subject–specific as inter–subject variability can be significant and such a validation is not optimal [11]. The objective of this work is to compare flow dynamics in realistic models of 5–year–old child and healthy male adult. The replicas of both models were used in experiments to validate obtained flow fields.

## 2. Material and methods

### 2.1. Models

A realistic replica of healthy human adult has been developed in the past [12]. The model was employed in properly validated numerical simulations [10]. To study the effect of age on flow dynamics the model was down–scaled to correspond to respiratory airways of 5–years–old child (Fig. 1.).

The down–scaling was executed in two steps. This is reasonable approach as there are differences in growth of different airway regions, e.g. mouth–throat region and conducting airways. Also, there are no studies that would include dimensions of both upper and lower pediatric airways. Considering inter–subject variability, it is not optimal to group data from various studies together. Moreover, different teams use different methologies and publish dimensions of different regions. Therefore, the tracheobronchial tree was down–sized with a scaling factor of 0.54 based on the trachea length [13]. After that, the upper respiratory airways were scaled down based on the length of the nasal cavity from nostrils to the end of septum [14]. The scaling factor of 0.8 was used which was slightly higher than average. The reason was that the head of the adult model was somewhat smaller than average and down–scaling of it based on the average dimensions would result in unrealistically small head for a 5–year–old child. The number of bronchial airways was decreased because of its small dimensions and 3D printing restrictions.

The child model was modified for the sake of experiments. A 2–mm–thick envelope was added around the model to permit a 3D printing of the model. A part of the trachea just upstream of the first bifurcation was substituted by a 1–cm–long glass tube (Fig. 2.). The cross section of this trachea part was approximately circular and therefore, the substitution with glass tube had minor effect on geometry. The inner diameter of the tube was carefully chosen to match the inner diameter of the trachea.

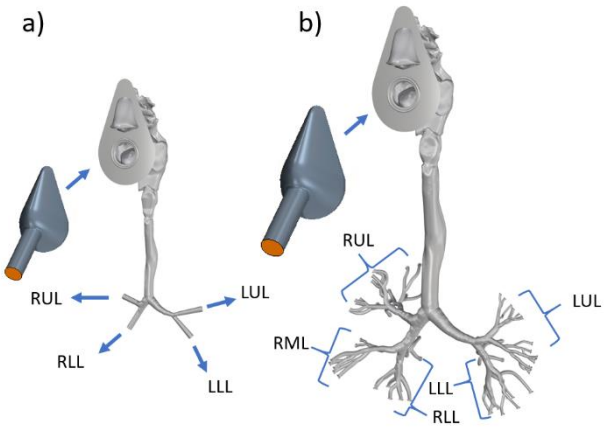


**Fig. 1.** Child (a) and adult (b) digital model of respiratory airways

A mask was created around the head to facilitate prescription of boundary conditions in the simulations and to permit hose connection during the experiments.

### 2.2. Numerical simulations

The digital geometries were imported into a commercial solver Star CCM+ version 2019.2 (Siemens PLM, Texas, USA). A computational grid consisting of polyhedral cells together with prism cells at the walls was generated. The first cell thickness at the wall was determined to satisfy the $y^+ < 1$ condition. Meshes containing $7.32 \cdot 10^6$ and $5.31 \cdot 10^6$ cells were selected for the child and adult geometry, respectively, based on a grid independency study.

A RANS k–ω SST turbulence model with low–Re corrections was used as a good trade–off between accuracy and computational costs. It proved to be able to capture mean–flow dynamics in the respiratory airway models reasonably well [15]. Moreover, this low–Reynolds–number model accurately predicted flows from low–level to high–level breathing spanning the range of Reynolds number from 500 to $10^4$ [16]. The pressure–velocity coupling was done using the SIMPLE algorithm. Linearized equations describing the air flow were solved according to the Gauss–Seidel iteration method.

The simulations were performed at steady state inhalation representing sedentary conditions. The total flow rate through the child model was 12.5 L/min based on the information in [17]. The flow division between different lung lobes was based on [18] and can be found in Table 1. The stationary inhalation of 15,1 L/min was chosen for the adult case and flow division into different outlets were selected according to [12]. It is worth noting that there is a constriction in left bronchi resulting in lower flow rate into the left lung compared to the average right/left lung flow ratio.

The pressure boundary condition was prescribed at the mask inlet and outward pointing velocities were set at the outlets in conformity with the experiments. The no–slip condition was assumed at the walls. The values of turbulent intensities at the inlets were set to 1 % and the value of ratio of turbulent viscosity to laminar viscosity was 10 %.

**Table 1.** Flow rates through respiratory airway models

| | child airways | adult airways |
|---|---|---|
| | flow rate (L/min) | |
| LUL | 3,16 | 1,7 |
| LLL | 2,58 | 2,8 |
| RUL | 2,61 | 3,4 |
| RLL | 4,15 | 3,4 |
| RML | | 3,8 |
| total | 12,5 | 15,1 |

### 2.3. Experimental measurements

LDA measurements (Fig. 2.) were carried out to validate CFD simulations. Velocities of a particle–laden flow were measured in several points in the trachea. A part of trachea was therefore substituted by a glass tube to provide optical access. Aerosol particles were generated in a condensational monodisperse aerosol generator TSI 3475 (TSI Inc., Shoreview,MN, USA) utilizing heterogeneous condensation of Di–Ethyl–Hexyl–Sebacate (DEHS) vapour on NaCL particles. The resulting particle size was measured using process aerosol monitor TSI 3375 (TSI Inc., Shoreview,MN, USA). The particle size was in a range of 2,5–3 μm to satisfy a Stokes number (Stk) < 0.1 condition to assure that particles closely follow the streamlines.

The flow through the model was driven by a vacuum pump. The flow division was set up by a flowmeter with regulating valve downstream of each outlet. A filter was inserted just upstream of each flowmeter to collect all the DEHS particles that penetrate the model.

2D LDA FlowExplorer (Dantec Dynamics A/S, Skovlunde, DK) was employed to measure point–wise velocities. The measurements were performed in several points in a coronal plane 10 mm above the first bifurcation. The LDA system contained two built-in diode pumped solid state lasers with wavelengths of 660 nm and 785 nm. The beam from each laser was split into two parallel beams with a separation distance of 60 mm and power of 30 mW. The beam crossing formed a measuring volume with dimensions of 0.1 × 0.1 × 0.8 mm. The wavelengths of 660 and 785 nm were utilized to measure the axial and radial velocity, respectively. The LDA system was used in a backscatter mode and had a lens focal length of 150 mm. The LDA signals were processed using a Dantec P80 processor and the data acquisition was controlled using BSA Flow software v5.2.

## 3. Results

### 3.1. CFD and experiments comparison

The obtained axial velocities by both experiments and simulations were compared (Fig. 3.). Both the methods agreed reasonably well. The experimental velocity towards the left wall (positive distance from the axis) decreased more rapidly and are less symmetrical compared to simulations. The size of the measurement volume also prohibited to measure velocities closer than 1 mm to the wall.

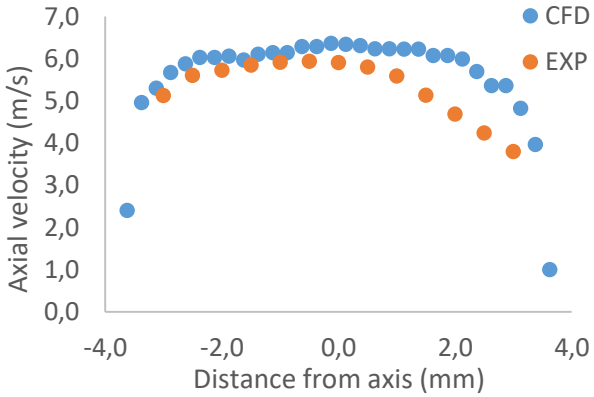


**Fig. 3.** Comparison of axial velocities obtained by CFD and LDA measurements. The velocities studied in coronal plane of the child airway model. Positive distance from axis corresponds to left side of the model.

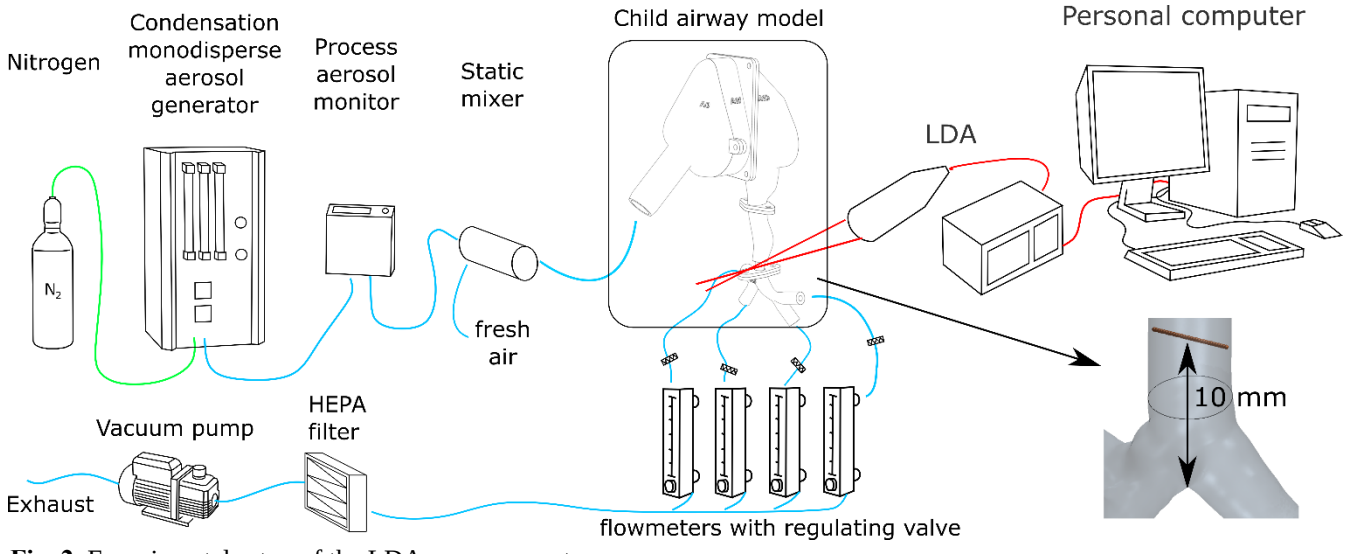


**Fig. 2.** Experimental setup of the LDA measurement

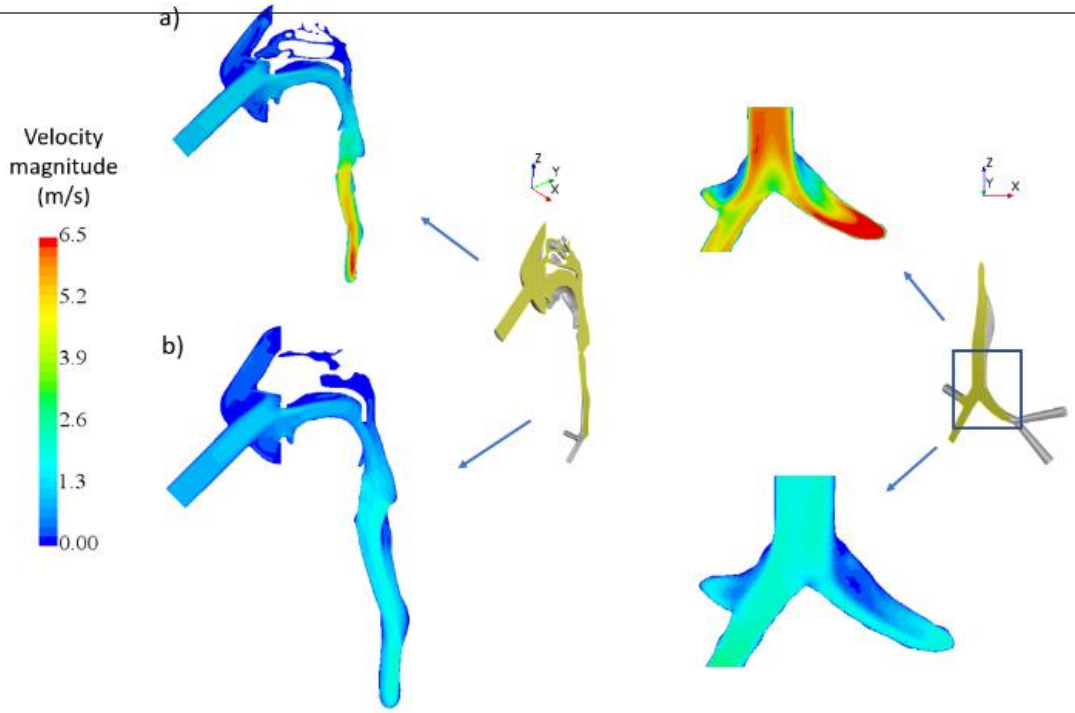


**Fig. 4.** Velocity magnitudes in sagittal and coronal plane of a) child and b) adult model

### 3.2. Child and adult airway flow dynamics comparison

Results of numerical simulations, in particular velocity magnitudes and wall shear stresses, are discussed below. Comparison of velocity magnitudes in sagittal and coronal plane are depicted in Fig. 4. The planes were created at the centreline of the first bifurcation. The Reynolds numbers ($\rho UD/\mu$) at the trachea inlet were 1913 and 1210 for the child and adult model, respectively, indicating the flow is in laminar regime. The velocity trends were similar in both the models. Majority of the air flowed through the mouth due to high pressure loss of the nasal cavity. The air in the trachea was skewed towards the front trachea wall because of the glottis geometry. Zones of flow reversal can be seen in daughter branches of the first bifurcation (right side of Fig. 4.)

The velocity magnitudes differed in the two models. The velocities were higher in the case of the child model compared to the adult case. The maximum velocities were approximately three times higher in the child model. This was caused by a significant increase in airway calibers and a small increase of inhalation flow rate comparing the child case to the adult one. The inhalation flow rate is affected by both respiratory rate and tidal volume.

The wall shear stress expresses a force exerted on the airway wall by a fluid motion. It is proportional to the velocity gradient next to the wall [19]. The wall shear stress distribution at the model walls is depicted in Fig. 5. It can be seen that the wall shear stress was high at the bifurcations and glottis area. The highest wall shear stress was in the left bronchi bifurcation. It is worth noting that the model encompasses a constriction in the left bronchi that generates high velocities. Comparing the models, the wall shear stress was higher in the child model. The

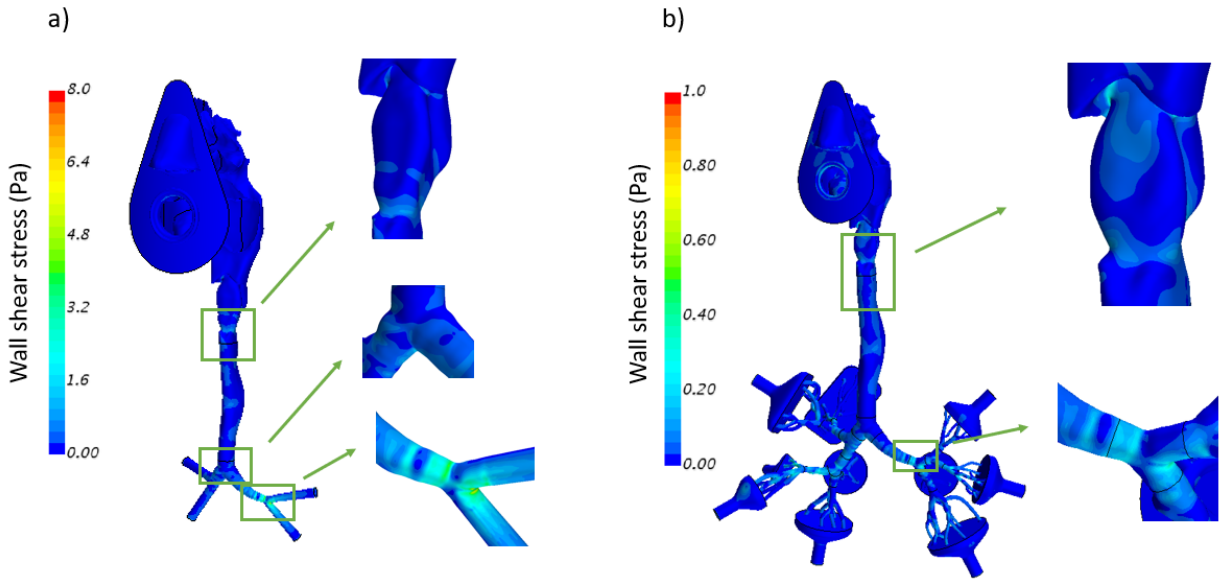


**Fig. 5.** Contours of wall shear stress in a) child and b) adult model

maximum values were 7.4 and 0.96 in the child and adult model, respectively. The strong forces exerted on the child airway walls by the fluid flow indicate their higher susceptibility to wall damages compared to adults.

## 4. Conclusions

The model of child airways was created by downscaling an adult model. The child model included upper respiratory airways and conducting airways down to 2nd generation. The model was employed in properly validated CFD simulations.

The LDA point–wise velocity measurements in the lower part of the trachea were carried out. The measured axial velocities were compared to the ones obtained from simulations. Reasonably good agreement was found.

The results of numerical simulations in the child model were compared to the ones from adult model. The velocity trends were similar, but the velocity magnitudes were higher in the child model. This was caused by a significant increase of airway calibres compared to small increase of inhalation flow rate from childhood to adulthood. Regions of increased velocity could result in enhanced particle deposition due to inertia and thus, higher risk for children inhaling polluted air.

The forces exerted on the airway walls by the flowing fluid, i.e. wall shear stresses, were studied in both the models. The zones of high wall shear stress corresponded to the zones of high velocities, e.g. glottis area or bifurcations. The maximum values of wall shear stress were 7.4 and 0.96 in the child and adult airways, respectively. The roughly eight-fold increase in the child airways compared to the adult ones indicate higher child vulnerability to wall damages.

**Acknowledgement.**This work was supported by the Czech Science Foundation under the grant GA20-27653S.

## References

1 UNICEF, *Clear the air for children*. (United Nations Children´s Fund, New York, USA, 2016).
2 D. A. Stern, W. J. Morgan, A. L. Wright, S. Guerra, and F. D. Martinez, Lancet **370** (9589), 758 (2007).
3 N. A. Clark, P. A. Demers, C. J. Karr, M. Koehoorn, C. Lencar, L. Tamburic, and M. Brauer, Environmental health perspectives **118** (2), 284 (2010).
4 I. Amirav and M. T. Newhouse, Expert Rev Respir Med **2** (5), 597 (2008).
5 J. X. Xi, X. H. Si, Y. Zhou, J. Kim, and A. Berlinski, Respiratory care **59** (2), 263 (2014).
6 J. M. Oakes, S. C. Roth, and S. C. Shadden, Annals of Biomedical Engineering **46** (3), 498 (2018).
7 P. Das, E. Nof, I. Amirav, S. C. Kassinos, and J. Sznitman, Plos One **13** (11) (2018).
8 E. G. Tsega, Comput Math Method M **2018** (2018).
9 Q. H. Deng, C. Y. Ou, J. Chen, and Y. G. Xiang, Sci Total Environ **612**, 339 (2018).
10 J. Elcner, F. Lizal, J. Jedelsky, M. Jicha, and M. Chovancova, Biomech Model Mechan **15** (2), 447 (2016).
11 C. Darquenne, W. J. Lamm, J. M. Fine, R. A. Corley, and R. W. Glenny, Journal of Aerosol Science **99**, 27 (2016).
12 F. Lizal, J. Elcner, P. K. Hopke, J. Jedelsky, and M. Jicha, Proceedings of the Institution of Mechanical Engineers Part H-Journal of Engineering in Medicine **226** (H3), 197 (2012).
13 M. H. Dave, M. Kemper, A. R. Schmidt, C. P. Both, and M. Weiss, Pediatr Anesth **29** (8), 782 (2019).
14 L. Golshahi, M. L. Noga, R. B. Thompson, and W. H. Finlay, Journal of Aerosol Science **42** (7), 474 (2011).
15 P. Koullapis, S. C. Kassinos, J. Muela, C. Perez-Segarra, J. Rigola, O. Lehmkuhl, Y. Cui, M. Sommerfeld, J. Elcner, M. Jicha, I. Saveljic, N. Filipovic, F. Lizal, and L. Nicolaou, European Journal of Pharmaceutical Sciences (2017).
16 C. Kleinstreuer and Z. Zhang, International Journal of Multiphase Flow **29** (2), 271 (2003).
17 M. Roy and C. Courtay, Radiation Protection Dosimetry **35** (3), 179 (1991).
18 N. Jahani, S. Choi, J. Choi, K. Iyer, E. A. Hoffman, and C. L. Lin, J Appl Physiol (1985) **119** (10), 1064 (2015).
19 B. Sul, A. Wallqvist, M. J. Morris, J. Reifman, and V. Rakesh, Comput Biol Med **52**, 130 (2014).